Functional Anticodon Architecture of Human tRNA^{Lys3} Includes Disruption of Intraloop Hydrogen Bonding by the Naturally Occurring Amino Acid Modification, t^{6}A†

John W. Stuart,[‡] Zofia Gdaniec,[§] Richard Guenther,[‡] Michal Marszalek,[||] Elzbieta Sochacka,[||] Andrzej Malkiewicz,[||] and Paul F. Agris*,[‡]

Department of Biochemistry, North Carolina State University, Raleigh, North Carolina 27695-7622, Institute of Bioorganic Chemistry, Polish Academy of Sciences, Poznan 61-704, Poland, and Institute of Organic Chemistry, Technical University, Lodz 90-924, Poland

Received June 6, 2000; Revised Manuscript Received September 1, 2000

ABSTRACT: The structure of the human tRNA^{Lys3} anticodon stem and loop domain (ASL^{Lys3}) provides evidence of the physicochemical contributions of *N*6-threonylcarbamoyladenosine (t^{6}A$_{37}$) to tRNA^{Lys3} functions. The t^{6}A$_{37}$-modified anticodon stem and loop domain of tRNA$^{Lys3}_{UUU}$ (ASL$^{Lys3}_{UUU}$- t^{6}A$_{37}$) with a UUU anticodon is bound by the appropriately programmed ribosomes, but the unmodified ASL$^{Lys3}_{UUU}$ is not [Yarian, C., Marszalek, M., Sochacka, E., Malkiewicz, A., Guenther, R., Miskiewicz, A., and Agris, P. F., *Biochemistry 3*9, 13390−13395]. The structure, determined to an average rmsd of 1.57 ± 0.33 Å (relative to the mean structure) by NMR spectroscopy and restrained molecular dynamics, is the first reported of an RNA in which a naturally occurring hypermodified nucleoside was introduced by automated chemical synthesis. The ASL$^{Lys3}_{UUU}$-t^{6}A$_{37}$ loop is significantly different than that of the unmodified ASL$^{Lys3}_{UUU}$, although the five canonical base pairs of both ASL$^{Lys3}_{UUU}$ stems are in the standard A-form of helical RNA. t^{6}A$_{37}$, 3′-adjacent to the anticodon, adopts the form of a tricyclic nucleoside with an intraresidue H-bond and enhances base stacking on the 3′-side of the anticodon loop. Critically important to ribosome binding, incorporation of the modification negates formation of an intraloop U$_{33}$·A$_{37}$ base pair that is observed in the unmodified ASL$^{Lys3}_{UUU}$. The anticodon wobble position U$_{34}$ nucleobase in ASL$^{Lys3}_{UUU}$-t^{6}A$_{37}$ is significantly displaced from its position in the unmodified ASL and directed away from the codon-binding face of the loop resulting in only two anticodon bases for codon binding. This conformation is one explanation for ASL$^{Lys3}_{UUU}$ tendency to prematurely terminate translation and −1 frame shift. At the pH 5.6 conditions of our structure determination, A$_{38}$ is protonated and positively charged in ASL$^{Lys3}_{UUU}$-t^{6}A$_{37}$ and the unmodified ASL$^{Lys3}_{UUU}$. The ionized carboxylic acid moiety of t^{6}A$_{37}$ possibly neutralizes the positive charge of A$^+_{38}$. The protonated A$^+_{38}$ can base pair with C$_{32}$, but t^{6}A$_{37}$ may weaken the interaction through steric interference. From these results, we conclude that ribosome binding cannot simply be an induced fit of the anticodon stem and loop, otherwise the unmodified ASL$^{Lys3}_{UUU}$ would bind as well as ASL$^{Lys3}_{UUU}$-t^{6}A$_{37}$. t^{6}A$_{37}$ and other position 37 modifications produce the open, structured loop required for ribosomal binding.

Lysine tRNAs with UUU anticodons have a conventional role in ribosome-mediated protein synthesis. In addition, tRNA$^{Lys}_{UUU}$ species facilitate −1 frameshifts for correct translation of the *E. coli* DNA polymerase γ subunit (*1*) and retroviral polymerases (*2*). Also, tRNA$^{Lys}_{UUU}$ often misreads asparagine codons (*3, 4*) and peptidyl-tRNA^{Lys} prematurely terminates translation more often than other tRNAs (*5*). In addition, reverse transcription of the HIV-1 genomic RNA is primed by the human tRNA$^{Lys3}_{UUU}$. Formation of the viral replication initiation complex is enhanced in vitro by the presence of the tRNA's modified nucleosides (*6, 7*) and strand transfer is facilitated by the anticodon's modified nucleosides (*8*). We hypothesized that anticodon domain modified nucleosides impart the unique chemical and structural properties required to explain the standard (*9*), as well as the unconventional, roles of tRNA$^{Lys}_{UUU}$ in protein synthesis and as primer for HIV replication (*10*).

Two posttranscriptional modifications in the anticodon loop distinguish tRNA$^{Lys}_{UUU}$ from other tRNA^{Lys} species and from other tRNAs, in general. In human tRNA$^{Lys3}_{UUU}$, position 34 is modified to 5-methoxycarbonylmethyl-2-thiouridine (mcm^{5}s^{2}U$_{34}$)[1] and A$_{37}$ is modified to 2-methylthio-*N*6-threonylcarbamoyladenosine (ms^{2}t^{6}A$_{37}$). There is only one lysine tRNA in *E. coli*, tRNA$^{Lys}_{UUU}$, and its anticodon stem and loop sequence closely resembles that of human tRNA$^{Lys3}_{UUU}$. In *E. coli* tRNA$^{Lys}_{UUU}$, U$_{34}$ and A$_{37}$ are modified to 5-methylaminomethyl-2-thiouridine (mnm^{5}s^{2}U) and t^{6}A, respectively. Posttranscriptional modifications of

[†] This research was supported by the National Science Foundation (MCB9631103 to P.F.A.), the Department of Health and Human Services (PHS NIH Grant GM-23027 to P.F.A.), Cambridge Isotope Laboratories, Inc. (P.F.A.), and the Polish Committee for Scientific Research Grant 0877/T09/96/11 (A.M.).

* To whom correspondence should be addressed. Phone: (919) 515-6188. Fax: (919) 515-2047. E-mail: Agris@bchserver.bch.ncsu.edu.

[‡] North Carolina State University.

[§] Polish Academy of Sciences.

[||] Technical University.

10.1021/bi0013039 CCC: $19.00
Published on Web 10/10/2000

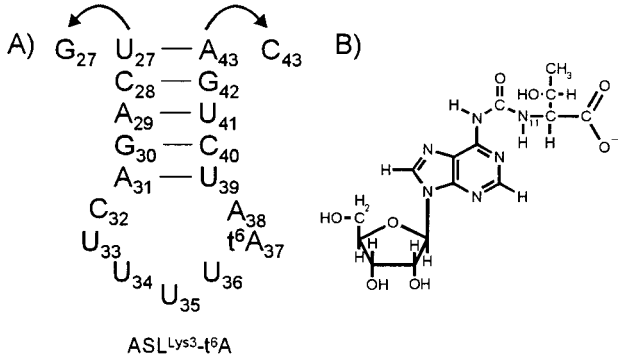

FIGURE 1: (A) Sequence and secondary structure of the tRNA$^{Lys3}_{UUU}$ anticodon stem/loop (ASL$^{Lys3}_{UUU}$) with the t^{6}A$_{37}$ modification. The molecule used for structure determination had the terminal base pair U$_{27}$·A$_{43}$ replaced with G$_{27}$·C$_{43}$. (B) The structure of t^{6}A$_{37}$ with the carboxylic acid of threonine dissociated (pH 5.6).

the tRNA$^{Lys}_{UUU}$ anticodon loop, but not those of the anticodon stem, are important for aminoacyl-tRNA synthetase recognition and aminoacylation of cognate tRNA (*11*) and for ribosomal binding (*12*, *13*). Recently, we determined that the individual modifications of the tRNA$^{Lys}_{UUU}$ anticodon loop, s^{2}U$_{34}$, mnm^{5}U$_{34}$ (of mnm^{5}s^{2}U$_{34}$) and t^{6}A$_{37}$, restored AAA-programmed ribosomal binding to the otherwise unmodified and nonfunctional human tRNA$^{Lys3}_{UUU}$ anticodon stem and loop domain (*13*, *14*, preceding paper in this issue).

Here we report the structure of the human tRNA$^{Lys3}_{UUU}$ anticodon stem and loop with the amino acid modification, t^{6}A$_{37}$ (ASL$^{Lys3}_{UUU}$-t^{6}A$_{37}$), which is critical to its ribosome binding function (*14*). Structures of the unmodified ASL$^{Lys3}_{UUU}$ and the stem modified ASL$^{Lys3}_{UUU}$-Ψ$_{39}$ have been reported (*15*), but neither bind the ribosome (*14*). We compare the structure of the functional ASL$^{Lys3}_{UUU}$-t^{6}A$_{37}$ to that of the nonfunctional, unmodified ASL$^{Lys3}_{UUU}$. The hypermodified nucleoside has a pronounced effect on the anticodon loop conformation as determined from NMR-derived distance and torsion angle restraints using restrained molecular dynamics. The structure explains the role of t^{6}A in achieving an anticodon architecture required for ribosome binding, as well as the unique properties displayed by tRNA$^{Lys}_{UUU}$ species.

EXPERIMENTAL PROCEDURES

Materials: Sample Preparation. The heptadecamer oligoribonucleotides corresponding to the unmodified and *N*6-threonylcarbamoyladenosine (t^{6}A$_{37}$)-modified sequence of the human tRNA$^{Lys3}_{UUU}$ anticodon stem and loop domain, ASL$^{Lys3}_{UUU}$ (Figure 1) were chemically synthesized using standard phosphoramidite chemistry on an Applied Biosystems 394 DNA/RNA Synthesizer (*16*). The 5′ to 3′ terminal base pair was changed from the native sequence Ψ$_{27}$·A$_{43}$ to G$_{27}$·C$_{43}$ for the increased yield and increased stability necessary for NMR analysis. The 5′-trityl-2′-dimethyltertbutylsilyl-3′-^{15}N3-uridine phosphoramidite was synthesized as previously described (*17*) and the protected 5′-trityl-2′-dimethyltertbutylsilyl-3′-phosphoramidite of t^{6}A was prepared in our laboratories (unpublished). All other nucleoside phosphoramidites were obtained from Glen Research (Sterling, VA). The oligomer was HPLC-purified as previously described (*17*) using a Nucleogen 60-7 DEAE (250 × 10 mm) column, and its nucleoside composition determined (*18*). Sample desalting was accomplished with Waters Corporation Sep-pak columns. The sample was prepared for NMR spectroscopy by extensive dialysis with buffer (10 mM cacodylate buffer, pH 5.6, 0.1 mM EDTA, 6% D$_2$O/94% H$_2$O) using Amicon Centricon 3 concentrators. For experiments in D$_2$O, the sample solution was evaporated down with N$_2$ and exchanged with D$_2$O three times before resuspending the sample in 99.96% D$_2$O. The samples used for structural analysis had a final RNA concentration of 1.2 mM.

Methods: (i) ASL Thermodynamic Parameters. ASL$^{Lys3}_{UUU}$ samples were dissolved to a concentration of 2 μM in either a phosphate or cacodylate buffer (10 mM sodium phosphate or 10 mM sodium cacodylate, 100 mM NaCl, 0.1 mM EDTA, with the pH adjusted with HCl). Thermal denaturations, performed in triplicate, were monitored by UV absorbance (260 nm) using a Cary 3 spectrophotometer as previously described (*19*). Data points were averaged over 20 s and collected three times a minute. Denaturations and renaturations were conducted over a temperature range of 5−90 °C and at three pH values (7.2, 6.0, and 5.0) with a ramp rate of 1 °C/min. Data from denaturations and renaturations were treated similarly. No hysteresis was observed. Thermodynamic parameters were calculated with a van't Hoff analysis of the data as described by Serra and Turner (*20*) using Origin software (Microcal). Substitution of the U$_{27}$·A$_{43}$ terminal base pair with a G$_{27}$·C$_{43}$ added stability to the molecule. A pH between 5.0 and 6.0 was deemed to be optimal for stability and pH 5.6 was chosen for NMR studies.

(ii) Unimolecular Property of Samples. To demonstrate that the RNA was a monomer at the NMR concentrations of this study, we measured the translational diffusion coefficient of the unmodified and t^{6}A$_{37}$-modified ASLs, and compared them to that of other RNA sequences of various lengths. This was accomplished with the pulsed field-gradient spin−echo technique (*21*, *22*), performed on the NMR sample itself, thereby obviating any complications or ambiguities of interpretation that may arise from approaches other than that by NMR methods (*23*). As would be expected for a monomer of this size, the translational diffusion coefficient of the heptadecamer was bracketed by those measured for a hexamer and a dodecamer, and by that of a 28-mer. Our results are in good agreement with published values of the translational diffusion coefficients of nucleic acids of similar sizes (*23*, *24*).

(iii) NMR Spectroscopy. All NMR spectra were collected on a Bruker DRX500 spectrometer and processed using either XWINNMR (Bruker Inc., Rheinstetten, Germany) or FELIX (Biosym/MSI, San Diego, CA). The residual water peak in D$_2$O samples was suppressed using low power presaturation whereas exchangeable proton resonances for samples in 94% H$_2$O/6% D$_2$O were collected at 1 °C with WATERGATE (*25*) solvent suppression. Eight one-dimensional spectra as a function of temperature between 4 and 31 °C and three

[1] Abbreviations: ASL, anticodon stem and loop domain; t^{6}A, *N*6-threonylcarbamoyladenosine; mcm^{5}s^{2}U, 5-methoxycarbonylmethyl-2-thiouridine; Ψ, pseudouridine; NMR, nuclear magnetic resonance; HPLC, high-performance liquid chromatography; DEAE, diethylaminoethyl; EDTA, ethylenediaminetetraacetic acid; NOE, nuclear Overhauser effect; NOESY, nuclear Overhauser effect spectroscopy; TOCSY, total correlation spectroscopy; HETCOR, heteronuclear correlation; HSQC, heteronuclear single quantum coherence; DQ, double quantum; DQF−COSY, double quantum filtered correlation spectroscopy; rmsd, root-mean-square deviation.

HSQC spectra at three pH values were obtained to aid signal assignments and assess protonation of A_{38}. NOESY spectra (*26*, *27*) used for analysis of the exchangeable protons were acquired with a mixing time of 150 ms. Spectra were acquired with sweep widths of 12019 Hz in both dimensions, 4096 points in t_2, and a minimum of 512 points in t_1 with 64 scans per increment.

Nonexchangeable protons were assigned using an assortment of two-dimensional spectra acquired at 10, 16, and 25 °C. NOESY spectra of the sample in D_2O had mixing times in the range of 50 to 400 ms. At least 256 points were collected in t_1, with 64 scans per increment. For these and the following homonuclear experiments, the spectral width was 6000 Hz in both dimensions, and 1024 points were collected in t_2. TOCSY (*28*) or clean TOCSY (*29*) experiments using the MLEV17 mixing sequence were performed at 16 °C with a mixing time of 60 ms. DQF−COSY (*30*) and double quantum (DQ) (*31*, *32*) experiments were obtained at 16 °C. The two-dimensional heteronuclear spectra that were collected included a $^1H-^{31}P$ HETCOR (*33*) and a hetero-TOCSY−NOESY (*34*). These spectra were all acquired at 16 °C. Natural abundance ^1H-^{13}C HSQC experiments (*35*−*37*) were performed at both 16 and 25 °C. For samples with site-specific ^{15}N labels, ^1H-^{15}N HSQC spectra were obtained in H_2O at 1 °C.

Distance restraints were derived from a series of phase sensitive NOESY spectra acquired with a 5000 Hz spectral width in both dimensions, 2048 points in t_2 and 512 points with 64 scans per block in t_1. Spectra were collected at 16 °C with mixing times of 50, 100, 140, 200, and 400 ms and processed (XWINNMR) with 60° phase-shifted sine bell apodization functions. The baseline in both dimensions was treated in FELIX using the FLATT algorithm (*38*). To provide suitable digital resolution for cross-peak integration, the spectra were zero-filled to 2048 by 1024 points.

(iv) Structure Determination. Distance restraints between nonexchangeable protons were obtained from the NOESY mixing time study. The NOE buildup curves were calculated by integrating the cross-peaks using FELIX and normalized by setting pyrimidine H5−H6 cross-peaks to a distance of 2.44 Å. Upper and lower bounds were set to the 20% above or below the calculated distance using flat-bottomed quadratic potentials. Cross-peaks with more than 35% overlap were classified strong (1.8−4 Å), medium (1.8−5 Å), or weak (1.8−6 Å) with large bounds to account for ambiguity of the peaks volume measurement. Threonine methyl protons of t^6A were handled as pseudo atoms and adjusted accordingly (*39*). The distance restraints involving exchangeable resonances were obtained from a single NOESY spectrum of the sample in 94% H_2O/6% D_2O. The cross-peaks were qualitatively classified as strong (1.8−3.5 Å), medium (1.8−4.5 Å), or weak (1.8−5.5 Å).

Dihedral angle restraints were placed on the δ backbone (C5′-C4′-C3′-O3′) to characterize the sugar puckers based on the $^3J_{H1'H2'}$ from the DQF−COSY spectrum. Observable H1′-H2′ cross-peaks with coupling constants less than 3 Hz were constrained to the C3′-*endo* conformation ($\delta = 85 \pm 30°$) while those with coupling constants greater than 7 Hz were constrained to the C2′-*endo* conformation ($\delta = 160 \pm 30°$). Sugars with intermediate coupling constants were left unrestrained. The α and ζ torsion angles were loosely constrained to exclude the trans conformation for those residues whose ^{31}P chemical shifts fell within the narrow range commonly seen for regular A-form structures (*40*, *41*). Last to better define the hydrogen-bonding pattern, distance restraints were added to the five base pairs in the stem and through-space dihedral restraints (±10°) were added to maintain planar bases.

Table 1: Thermodynamic Parameters[a] for ASL^{Lys3} Constructs

ASL construct	pH	T_m (°C)	ΔG_{37} (kcal/mol)[b]	ΔH (kcal/mol)	ΔS (cal/mol K)
ASL^{Lys3}_{UUU} unmodified	7.2[c]	57.5	−3.4	−55.4	−168
	6.0	61.6	−4.2	−57.8	−172
	5.0	56.3	−3.5	−60.6	−184
ASL^{Lys3}_{UUU}-t^6A_{37}	7.2[c]	54.7	−2.7	−49.5	−151
	6.0	60.2	−3.5	−50.6	−151
	5.0	58.4	−3.1	−48.0	−143

[a] Error in determinations: T_m, ±0.9 °C; ΔG_{37}, ±0.4; ΔH, ±3.0; ΔS, ±7. [b] ΔG_{37} determined at 37 °C. [c] Also cited in the preceding paper in this issue (*14*).

Structure calculations were preformed using InsightII (MSI) and protocols of Varani and others (*40*, *42*). To achieve the global fold of the molecule, 50 initial distance geometry structures were generated from a matrix of random trial distances derived from covalent bonds, distance, dihedral angle, and chiral restraints. The resulting structures were regularized as part of the distance geometry protocol by simulated annealing using the default settings in InsightII. For the refinement phase, the AMBER force field (*43*) was used with the standard nucleoside parameters except for the modified nucleoside t^6A_{37} and adenosine protonated at the 1 position (A^+_{38}). The state of t^6A at pH 5.6 with the carboxylic acid dissociated (*44*−*46*) was used to determine its partial charges, which were calculated from scaled MOPAC charges (*47*, *48*). Its atom types were derived by merging the existing AMBER atom types for adenine with that of threonine (*43*). The set of 50 distance geometry structures was heated to 2000 K for 5 ps with a 0.5 fs time step. During this equilibration step, the dihedral and chiral restraints ($k_{diheral} = 50$ kcal mol^{-1} rad^{-2}, $k_{chiral} = 25$ kcal mol^{-1} rad^{-2}) were scaled from 10% to their full value while the distance restraints remained at 50 kcal mol^{-1} Å^{-2}. Next, the structures were cooled from 2000 to 100 K over 25 ps with a time step of 0.5 fs during which all restraints were maintained at their full values. Longer simulation times did not improve the convergence of the lowest energy structures.

RESULTS

Thermodynamic Parameters. The anticodon stem and loop domain of human $tRNA^{Lys3}_{UUU}$, ASL^{Lys3}_{UUU} (Figure 1), was chemically synthesized with and without the threonine-modified adenosine *N*6-threonylcarbamoyl-adenosine, t^6A_{37}. At pH 7.2, the unmodified ASL^{Lys3}_{UUU} had a significantly higher melting temperature ($T_m = 57.5$ °C) and enhanced overall stability ($\Delta G = -3.4$ kcal/mol) than the ASL^{Lys3}_{UUU}-t^6A_{37} ($T_m = 54.7$ °C and $\Delta G = -2.7$ kcal/mol) (Table 1). Interestingly, the introduction of t^6A_{37} made a significant contribution to ΔS, though the T_m of the RNA had decreased. The two RNAs exhibited greater stability at pH 6 than at pH 7.2 or pH 5.0 (Table 1 and ref *14*). The increased stability and NMR-derived solution structures of the unmodified and Ψ_{39}-containing heptadecamers at low pH had already been reported and attributed to a $C_{32}\cdot A^+_{38}$ base pair (*15*). At the

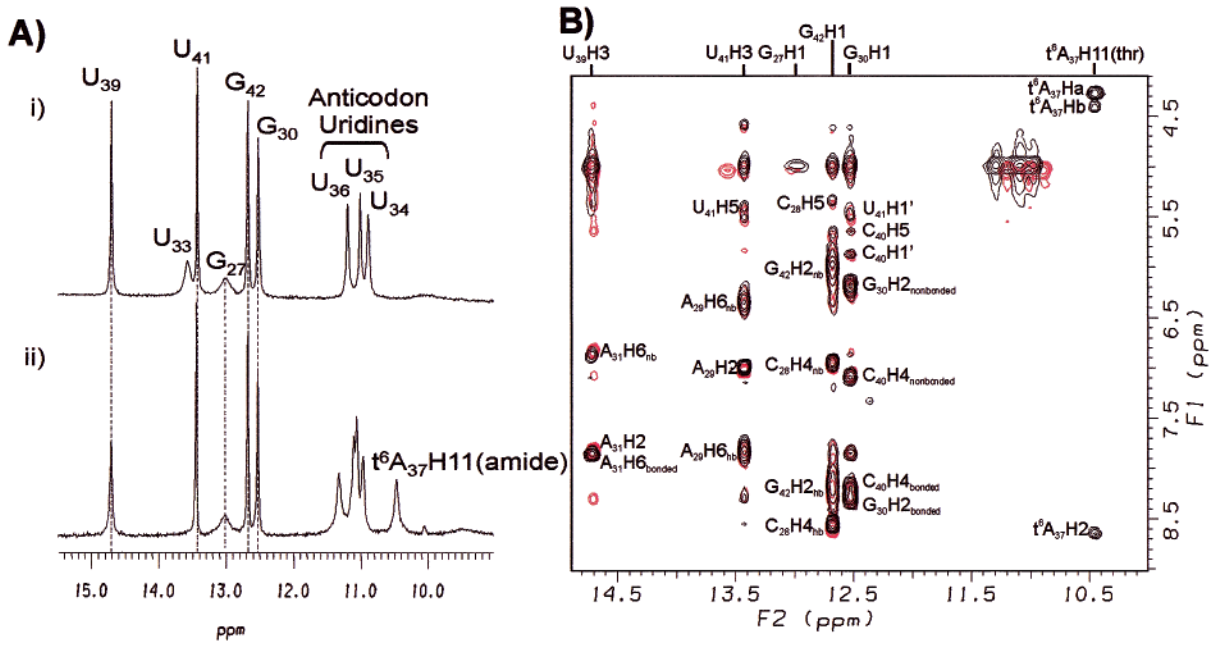

FIGURE 2: Comparison of exchangeable proton spectra of ASL$^{Lys3}_{UUU}$-t^{6}A$_{37}$ with that of the unmodified ASL$^{Lys3}_{UUU}$. (A) One-dimensional ^{1}H spectra in H_2O of ASL$^{Lys3}_{UUU}$-t^{6}A$_{37}$ (i) and unmodified ASL$^{Lys3}_{UUU}$ (ii). Iminos involved in base pairing in the stem are shown with dashed lines. (B) Overlay of the two-dimensional H_2O NOESY spectra of the imino region with ASL$^{Lys3}_{UUU}$-t^{6}A$_{37}$ shown in black and the unmodified ASL$^{Lys3}_{UUU}$ shown in red.

lower pH 5.0, protonation of Cs destabilizes the RNAs. Thus, we determined the ASL$^{Lys3}_{UUU}$-t^{6}A$_{37}$ structure at pH 5.6 by NMR spectroscopy and restrained molecular dynamics.

Assignment of Exchangeable Resonances. The one-dimensional and NOESY spectra of the unmodified and modified ASLs in H_2O revealed that the ASL$^{Lys3}_{UUU}$-t^{6}A$_{37}$ was stable and had a single predominant conformation (Figure 2). Sequential imino−imino connectivities for the stem were observed, indicating that the RNA adopted a folded structure. As is often the case, however, due to fraying, these sequential connectivities did not extend to the terminal base pair, G$_{27}$·C$_{43}$. The broad signal of the base-paired G$_{27}$ was visible in both the one-dimensional and NOESY spectra (Figure 2). In addition to the imino resonances of the stem, t^{6}A$_{37}$ H11, corresponding to the amide NH of threonine, had cross-peaks to the amino acid's Hα and Hβ and the purine's H2 (Figure 2B). This is the pattern one would expect with a side-chain coplanar to the parent base (*49*, *50*) and results in the modified nucleoside adopting the form of a tricyclic base. When the NOESY spectrum of the imino to amino region of the ASL$^{Lys3}_{UUU}$-t^{6}A$_{37}$ was compared to that of the unmodified sequence, a very similar pattern of resonance cross-peaks (except that contributed by t^{6}A) was observed with very little change in the chemical shifts. Likewise, comparison of other parts of the spectrum showed small changes in the chemical shifts of the resonances assigned to the stem, but considerably larger differences to the loop resonances. Cross-peaks observed in the imino to imino, and imino to amino, aromatic, and H1′ regions of the spectra were those expected of right-handed, helical nucleic acids (*35*, *51*). This implies that the t^{6}A$_{37}$ modification did little to perturb the stem of the hairpin, but significantly affected the conformation of the loop region. At pH 5.6, the N1 of A$_{38}$ is protonated in the unmodified ASL$^{Lys3}_{UUU}$ (*15*). Though this imino proton may be involved in a hydrogen bond with C$_{32}$ and thereby increase stability as was observed in thermal denaturation studies at pH 6 compared to 7.2, it was not directly observable by NMR. However, a pH dependent change in the chemical shift of the A$_{38}$H2, indicative of the protonation of the base (*15*), was observed in HSQC (^{1}H-^{13}C) spectra of both the unmodified ASL$^{Lys3}_{UUU}$ and ASL$^{Lys3}_{UUU}$-t^{6}A$_{37}$. Thus, introduction of t^{6}A$_{37}$ did not affect protonation of A$_{38}$.

While most signals of the spectra could be assigned using standard protocols, site-specific substitutions of ^{15}N-labeled nucleosides of the unmodified ASL$^{Lys3}_{UUU}$ were used to confirm or to identify the imino proton resonances of the uridine-rich loop. We were able to unambiguously identify the imino protons of loop residues U$_{34,}$ U$_{35}$ and U$_{36}$ (Figure 2A). Comparison of the one-dimensional spectra of the t^{6}A$_{37}$-modified and unmodified hairpin indicated a major rearrangement of the loop uridines with the introduction of t^{6}A$_{37}$. In the one- and two-dimensional spectra of the unmodified ASL$^{Lys3}_{UUU}$, a base-paired imino resonance at 13.55 ppm was assigned to U$_{33}$. This was the only imino proton unaccounted for by standard and ^{15}N-labeling procedures. Its position in the spectrum was that of a canonical U·A base pair that we assigned to U$_{33}$·A$_{37}$ in the unmodified ASL. However, the signal was not observed in spectra of ASL$^{Lys3}_{UUU}$-t^{6}A$_{37}$. Instead, a fourth free-imino signal from a uridine was observed between 10.9 and 11.4 ppm. This is the expected result from modification of the exocyclic amine of A$_{37}$ because t^{6}A$_{37}$ would be unable to form a canonical base pair with U$_{33}$. Thus, the introduction of t^{6}A$_{37}$ negated an intraloop U$_{33}$·A$_{37}$ base pair that was observable in the unmodified ASL$^{Lys3}_{UUU}$. Loss of the intraloop base pair was probably responsible for the lower T$_m$ of ASL$^{Lys3}_{UUU}$-t^{6}A$_{37}$, relative to that of the unmodified ASL$^{Lys3}_{UUU}$ (Table 1).

Assignment of Nonexchangeable Resonances. Assignment of the nonexchangeable resonances relied on a variety of homo- and heteronuclear experiments. Initial assignment of the aromatic H5−H6 protons relied on assigned nonex-

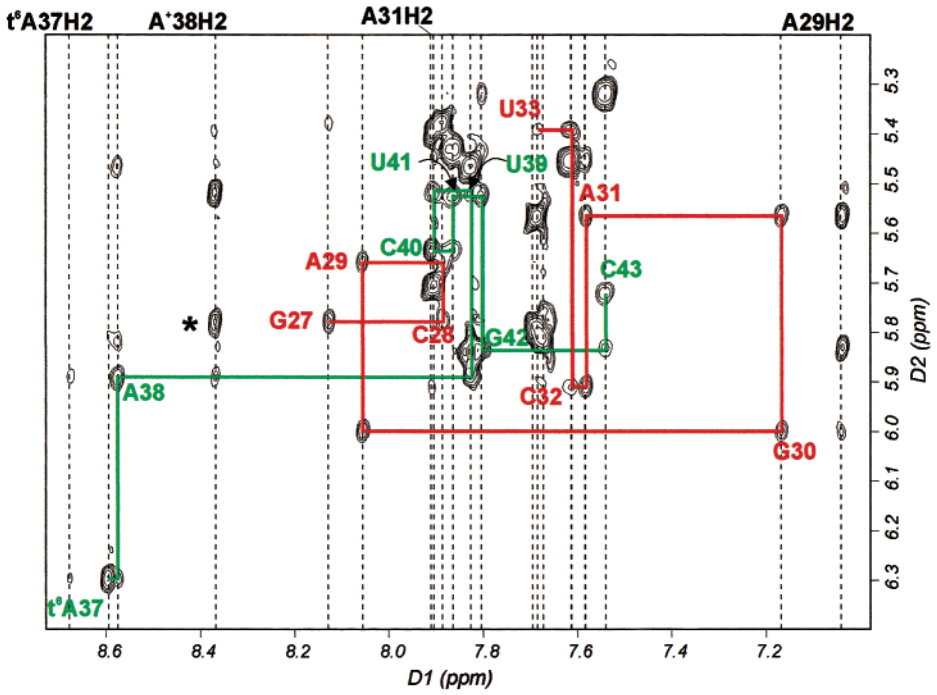

FIGURE 3: NOESY spectrum of ASL^{Lys3}_{UUU}-t^6A_{37} in D_2O at 25 °C showing connectivity between the aromatic protons and the H1′ of the ribose. The 5′ side of the loop is shown in red and the 3′ side of the loop is in green. Vertical dashed lines indicate each of the aromatic resonances, H8, H6, or H2. One of the important intraloop cross-peaks, A^+_{38}H2/U_{34}H1′ is marked with an asterisk.

changeable resonances and both DQF−COSY and TOCSY experiments. Differentiation of cytidine from the uracil aromatic protons was aided by natural abundance ^{1}H-^{13}C HSQC spectra. Cross-peaks from HSQC spectra were used to identify H1′ protons and distinguished adenosine H2 from purine H8 and pyrimidine H6 resonances. Both adenosines in the stem (A_{29} and A_{31}) had NOE cross-peaks from H2 to the H1′ proton of their 3′ neighbor and A_{29} also had an interstrand cross-peak to the H1′ of the 5′-adjacent base pair. Comparison to NOESY spectra of the sample in H_2O enabled us to assign the adenosine H2 resonances. Sequential aromatic-H1′ connectivities of the NOESY spectrum (in D_2O) could be traced for most of the molecule (Figure 3). As in the stem, A_{38} and t^6A_{37} stacked as indicated by NOEs to the H1′ of their 3′ neighbor. Several unique cross-peaks were also observed. There was a cross-peak from the t^6A_{37}-H2 to the methyl of the side chain (Hγ) and an unexpected NOE from A_{38}H2 across the loop to both H1′ and H2′ of C_{32}. Sequential aromatic-H1′ connectivities could be traced from the 5′ terminus of the stem to the first residue of the loop, C_{32} (Figure 3). At that point there was a break in the sequential connectivity that included the invariant U_{33}. Though NOEs were observed between U_{35} and U_{36}, sequential aromatic to H1′ connectivities began again at t^6A_{37} and continued to the 3′-terminal C_{43} (Figure 3). In the longer mixing time NOESY spectrum (400 ms), sequential connectivities between the nucleobase aromatics (H6, H8) were observed. These connectivities were apparent on the 5′ side of the stem from G_{27} to A_{31} and on the 3′ side of the loop from t^6A_{37} up to the 3′ terminus, with one exception. The chemical shift of C_{40}H6 was too close to its neighbors to be resolved reliably from the diagonal. Similar to the lack of aromatic to H1′ connectivities, no sequential aromatic-to-aromatic resonances were observed from residue A_{31} through t^6A_{37}.

Identification of three uridine nucleoside spin systems of the anticodon (U_{34}, U_{35}, U_{36}) was hindered by overlap in the spectra and a lack of resolvable intraresidue aromatic to ribose NOEs. Several long distance NOEs from already identified nucleosides in the loop to anticodon uridines were chosen for distance geometry analysis to determine the most likely uridine spin system assignment. A set of distance geometry calculations was performed with all assigned distance restraints and one interresidue restraint from an assigned resonance to an unassigned uracil. Then 60 structures were generated with three distance restraint sets (e.g., from A_{38}H2 to either U_{34}H1′, U_{35}H1′, or U_{36}H1′). After steepest decent minimization, the sets of structures were evaluated based on their total energy and magnitude of restraint violations. Assignment of an NOE to a particular anticodon uridine spin system was accomplished by eliminating those possibilities that yielded highly distorted geometries or high-energy structures.

Both DQF−COSY and TOCSY experiments were used to assign H1′ and H2′ resolvable cross-peaks. H1′−H2′ cross-peaks in the DQF−COSY spectrum were observed for loop residues, U_{33} to t^6A_{37}, and for C_{43}. The most intense H1′/H2′ cross-peaks were residues U_{33} to U_{36}. A short mixing time (50 ms) NOESY spectrum also aided in determining H2′ resonances. The H3′ of the riboses were assigned using the above spectra and the ^{1}H-^{31}P HETCOR spectrum. The same experiments were used to determine more than half of the H4′ and H5′/5″ protons.

NOE and Dihedral Angle Restraints. A total of 272 distance and dihedral angle restraints were used in the structure calculations (Table 2). Of the 220 NOE-derived restraints, there were 117 intranucleotide and 103 internucleotide distance restraints. Thirteen restraints were derived from exchangeable proton spectra and were added to mimic the hydrogen-bonding pattern of the stem and to limit fraying

Table 2: Structure Determination Statistics

total NOE distance restraints	220
intranucleotide NOEs	117
internucleotide NOEs	90
hydrogen-bonded stem base pairs	13
dihedral angle restraints	52
refinement statistics (10 lowest-energy structures)	
NOE violations (>0.1 Å)	0
dihedral angle violations (>10°)	0
avg pair wise rmsd (all heavy atoms) (Å)	
all residues	2.30 ± 0.67
stem residues (27−31,39−43)	0.76 ± 0.20
loop residues (32−38)	3.07 ± 1.07

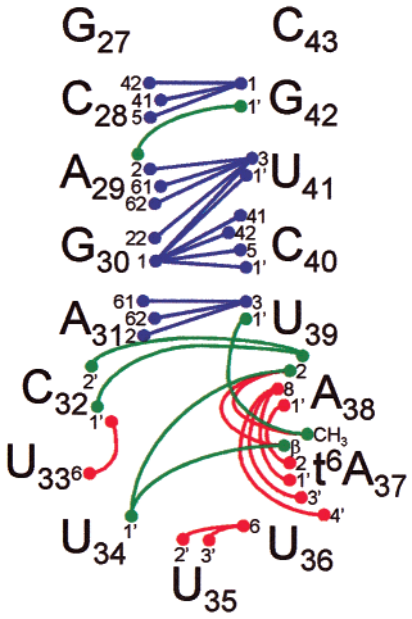

FIGURE 4: Illustration of a portion of the distance restraints used to determine the structure of ASL$^{Lys3}_{UUU}$-t^{6}A$_{37}$. Restraints derived from exchangeable resonances are depicted in blue while long-range (2 or more residues apart) restraints calculated from nonexchangeable NOE buildup curves are shown in green. Sequential distance restraints between bases are only shown for the loop residues (C$_{32}$·A$^+_{38}$) and are in red.

of the terminal bases (Table 2). In addition, a total of 52 dihedral angle restraints were used for structural calculations. From the DQF−COSY and ^{31}P spectra, 46 dihedral angle restraints defining the backbone and sugar pucker were incorporated. The torsion angles between U$_{33}$ and U$_{34}$ were left unrestrained to not bias the possibility of a tRNA^{Phe} anticodon-like U-turn, though none was observed in the ^{32}P-spectra of either the unmodified or t^{6}A$_{37}$-containing ASLs. In addition, five through space dihedral angle restraints were placed between the bases of the stem to maintain their planarity (±10°) and an additional restraint was needed on the side chain of t^{6}A$_{37}$ to keep it planar. The glycosidic angles χ were left unrestrained since the intranucleotide H1′/H6 or H1′/H8 NOE is capable of defining their syn/anti conformation. However, the long-range restraints, some of which are illustrated in Figure 4, were more informative and certainly more important in determining the global fold of the molecule. In particular, the distance restraints between the 5′ side of the stem and C$_{32}$ with A$_{38}$ and the threonine of t^{6}A$_{37}$ with A$_{38}$ and U$_{39}$ of the 3′-side of the stem were critical in defining the stem to loop angle of the ASL. The δ torsion angles for 14 residues were constrained based on the analysis of a high-resolution DQF−COSY spectrum. Residues U$_{33}$, U$_{34}$, and U$_{36}$ had H1′−H2′ coupling constants greater than 7 Hz and therefore were constrained to the C2′-endo range. In contrast, the stem residues had narrow H1′−H2′ (<2 Hz) cross-peaks, and were constrained to the C3′-endo range. Where the H3′−H4′ cross-peaks could be easily identified, a large coupling constant was observed. Residues with intermediate coupling constants, U$_{35}$, t^{6}A$_{37}$, and A$^+_{38}$, were left unconstrained. On the basis of the ^{31}P chemical shifts of all residues, their corresponding α and ζ torsion angles were loosely constrained to exclude the trans conformation, with the exceptions of U$_{33}$ and U$_{34}$, which were left unrestrained.

Structural Determination Features. A superposition of the 10 lowest energy structures of the ASL$^{Lys3}_{UUU}$-t^{6}A$_{37}$ resulted in an average pairwise rmsd of 2.30 ± 0.67 Å for all heavy atoms of the molecule (Figure 5A). The five base paired stem of ASL$^{Lys3}_{UUU}$-t^{6}A$_{37}$ adopted the form of A-RNA, and all stem nucleosides of the 10 lowest energy structures were C3′-endo. Only U$_{33}$, U$_{34}$, and U$_{36}$ of the loop were found to be strongly C2′-endo. Sixteen glycosidic angles were found to be anti, though no torsion angle restraints were used. Relative to the mean structure, the average rmsd was 1.57 ± 0.33 Å. The stem was much better defined than the loop. The heavy atom average pairwise rmsd of the stem was 0.76 ± 0.20 Å, while that of the loop was 3.07 ± 1.07 Å. Relative to the mean structure, the average rmsd was 0.52 ± 0.14 Å and 2.13 ± 0.52 Å for the stem and loop, respectively. The better rmsd relative to the average structure reflects that there were two somewhat different families of low energy structures. One family had U$_{33}$ stacked below C$_{32}$ while the second group of structures had U$_{33}$ placed adjacent to U$_{34}$. Similarly in determination of the structure of another seven-membered loop, that of the yeast tRNA^{Phe} TΨC loop, we found two almost equally populated families of structures with m^{5}U$_{54}$ (T$_{54}$) either within the loop or displayed outwardly (*42*). The H8/H1′ NOE between C$_{32}$ and U$_{33}$ in ASL$^{Lys3}_{UUU}$-t^{6}A$_{37}$ is weaker than an H8/H1′ internucleotide NOE for A-form RNA. With U$_{33}$ being the terminal base in the stacking on the 5′ side of the stem, weak base stacking could best account for the weaker NOE. For structure comparisons, we used a minimized average of the structures with C$_{32}$ and U$_{33}$ stacked (Figure 5B).

RNA hairpins have an angle between the plane of the loop and the axis of the stem that can only be defined by structural restraints between the loop and stem. A number of NOE cross-peaks are derived from C$_{32}$ on the 5′-side of the loop and t^{6}A$_{37}$ and A$_{38}$ on the 3′-side of the loop with the adjacent A$_{31}$−U$_{39}$ stem base pair. Restraints from these NOEs structure the loop locally at the junction with the stem (Figure 5C) in an angle of 133°, comparable to the 113° of the yeast tRNA^{Phe} X-ray crystallographic structure (*52*). In addition, RNA loops can be flexible and unstructured, particularly in the middle of the loop and when the loop is as large as that of the anticodon domain. The ASL$^{Lys3}_{UUU}$-t^{6}A$_{37}$ has a seven-membered loop typical of anticodon domains, but with four uridines in the middle of the sequence. Significant chemical shift similarities of these four tandem uridines (U$_{33}$, U$_{34}$, U$_{35}$, and U$_{36}$) made structure determination particularly challenging. However, ^{15}N-labeling and reiterative modeling allowed us to distinguish the uridines spin systems. A total of 69 NOE-derived distance and 16 backbone torsion angle

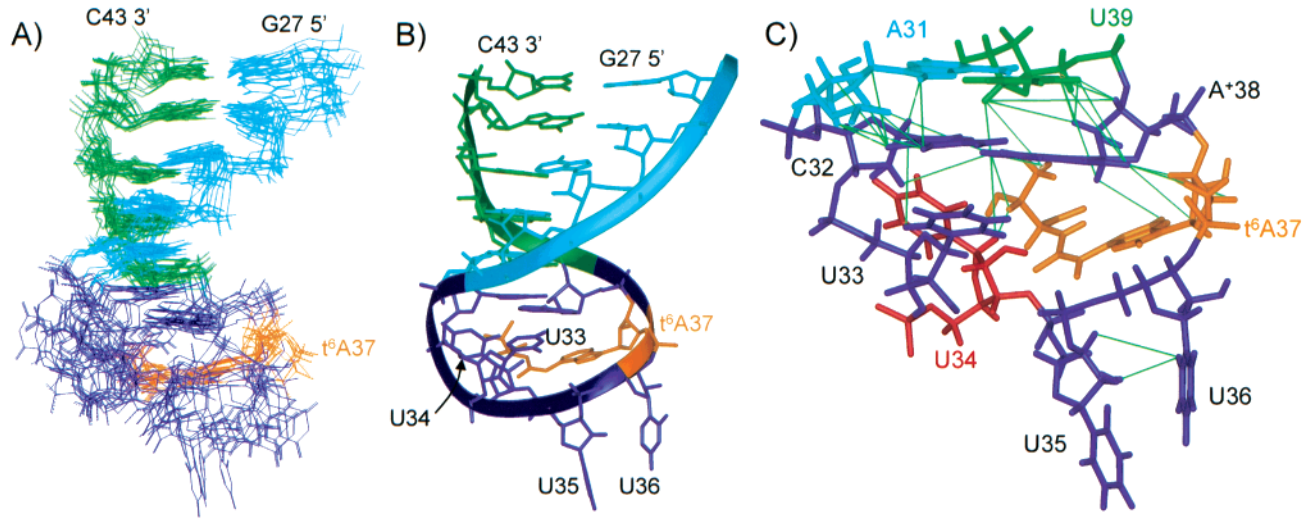

FIGURE 5: NMR derived structure of ASL^{Lys3}-t^6A_{37}. The 5′-side of the stem is shown in green and 3′-side shown in cyan; t^6A_{37} is highlighted in orange. (A) The superposition of 10 lowest energy structures of ASL^{Lys3}_{UUU}-t^6A_{37}. (B) Minimized average structure of the family where U_{33} stacks with C_{32}. (C) A close up view of the nucleosides at the base of the stem and the loop of ASL^{Lys3}_{UUU}-t^6A_{37} with U_{34} shown in red for clarity. Hydrogen atoms are displayed with green lines indicating interresidue NOEs.

restraints defined the loop structure and some of the distance restraints are shown in Figure 5C. NOEs limited the positions of the anticodon nucleosides. NOEs from U_{34} to A^+_{38} and t^6A_{37} restrained U_{34} to a position in the loop (Figure 5C). U_{34} in the unmodified ASL^{Lys3}_{UUU} structure also is located in the loop and away from the other anticodon uridines (*15*), though its position is different from that in the t^6A_{37}-modified ASL^{Lys3}_{UUU} (Figure 6). In contrast, Gm_{34} in the purine-rich anticodon of the X-ray crystallographic structure of yeast $tRNA^{Phe}$ is stacked with the subsequent anticodon bases (*52*). Also in contrast to yeast $tRNA^{Phe}$, the lack of any far shifted resonances in the phosphorus spectrum suggests that there is no U-turn found in ASL^{Lys3}_{UUU}-t^6A in solution. The signature cross-peak of a U-turn, the *n* to *n* + 2 internucleotide H1′ to H8 resonance, was not observed due to overlap in the NOESY spectra. Although we did not eliminate the possibility of a U-turn in the dihedral restraints, no structures with U-turns were generated. In fact, U_{34} could not have NOEs with A^+_{38} and t^6A_{37} and remain at the bottom of the anticodon loop as in yeast $tRNA^{Phe}$.

DISCUSSION

Incorporation of t^6A_{37} into the otherwise unmodified and nonfunctional ASL^{Lys3}_{UUU} restored ribosome-mediated, poly-A binding (*14*, preceding paper in this issue). Because the physicochemical contributions of t^6A_{37} impart function to the ASL, it was important to determine the ASL^{Lys3}_{UUU}-t^6A_{37} structure and define the differences in conformation between it and the unmodified ASL. The structures of the unmodified ASL^{Lys3}_{UUU} and ASL^{Lys3}_{UUU} with Ψ_{39} in the stem and immediately adjacent to the loop (*15*) are pertinent to the description of the ASL^{Lys3}_{UUU}-t^6A_{37} structure. The presence of pseudouridine demonstrably stabilized the conformation (*14*, *15*). However, we have found that both the unmodified and Ψ_{39}-containing ASL^{Lys3}_{UUU} are nonfunctional, i.e., the ASL constructs will not bind poly-A programmed ribosomes (*14*, preceding paper in this issue).

The addition of t^6A_{37} to the 3′-side of the loop and adjacent to the anticodon of ASL^{Lys3}_{UUU} altered the structure of the molecule in a way that allowed it to bind the ribosome (*14*, preceding paper in this issue). Examination of the exchangeable NOESY spectra shows that t^6A_{37} does not change the conformation of the stem. Thus, t^6A's physicochemical contribution to a rearrangement of the loop results in the ASL's AAA codon binding activity. In the unmodified ASL,

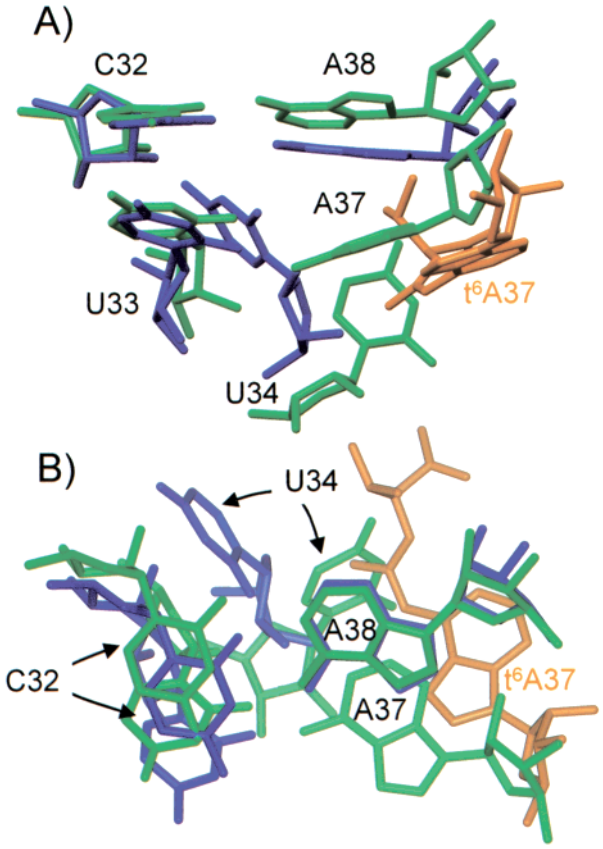

FIGURE 6: Superposition of the ASL^{Lys3}_{UUU}-t^6A_{37} (blue) and unmodified ASL^{Lys3}_{UUU}-(U_{27}·A_{43}) (green) (*15*). Phosphate atoms were used to superimpose the structures. The ribose and phosphate backbone along with U_{35} and U_{36} are not displayed to improve clarity. (A) Side view showing U_{34} displacement by the threonyl modification of t^6A_{37}. (B) Top view showing that the new position of U_{34} displaces C_{32}.

there is a potential Watson−Crick base pair between U_{33} and A_{37}. An upfield, exchangeable, imino proton resonance, assigned to this base pair in the unmodified ASL^{Lys3}_{UUU}, was not evident in spectra of the t^6A_{37}-modified ASL^{Lys3}_{UUU}. Thus, the threonyl modification on t^6A_{37} negates the possibility of this intraloop base pair resulting in an overall lower melting temperature (Table 1). An overall lowering of the melting temperature was observed when t^6A_{37} was incorporated into the anticodon stem and loop of the isoaccepting $tRNA^{Lys1,2}_{CUU}$ species differing in sequence only by a C_{34} and an inversion of the stem's C_{28}·G_{42} base pair (*14*, preceding paper in this issue). We had predicted these results when we hypothesized that one function of position 37 modifications was to inhibit canonical intraloop base pairs in order to maintain an open anticodon loop (*9*).

The seven-membered anticodon loop could be envisioned as a point of structural dynamics in the tRNA molecule, and a region in which stacking interactions would not be found. However, hydrogen bonding between t^6A_{37} H11 and N1 of the threonyl side chain of t^6A_{37} completes an additional planar ring on adenosine and consequently makes it similar to the guanosine-derived, tricyclic base wybutosine-37 of yeast $tRNA^{Phe}$. The tricyclic nature of t^6A possibly enhances the base stacking ability of the nucleoside. In the solution structure of the ASL^{Lys3}_{UUU}, t^6A_{37} and A^+_{38} are coplanar and stacked but because the threonyl side chain must be accommodated in the loop, the two bases are offset by an angle of 40.1°. Stacking interactions are very important in stabilizing RNA structures. Calculations of the entropic thermodynamic parameter (ΔS) for the t^6A_{37}-modified and unmodified ASL^{Lys3}_{UUU} (Table 1), and for the anticodon stem and loop of the isoaccepting $tRNA^{Lys1,2}_{CUU}$ species (*14*, preceding paper in this issue), indicate a considerable contribution by t^6A_{37}. In all structures of all calculations, t^6A_{37} is stacked on A_{38}, which is in turn stacked on the adjacent U_{39} in the stem. Thus, modification at position 37 structures the 3′-side of the loop with stacking to A_{38} and the adjacent stem.

t^6A_{37} displaces U_{34} relative to its position in the unmodified ASL. However, U_{34} in proximity to A^+_{38} and t^6A_{37}, this leaves only two residues, U_{35} and U_{36} available for hydrogen bonding to a message on the ribosome (Figure 5). With only two of three anticodon bases available for codon pairing, this unconventional anticodon structure is a reasonable explanation for the bacterial and mammalian $tRNA^{Lys}_{SUU}$ tendency to frame shift, prematurely terminate translation and mis-read Asn codons (*10*). We postulated that the modified nucleoside distortion of the anticodon loop was a possible structural determinant for the preferential selection of $tRNA^{Lys3}_{SUU}$ as primer of HIV-1 reverse transcriptase in vivo (*10*). U_{35} and U_{36}, though not well defined in the structure for lack of NOE restraints to other nucleosides, were displayed outward from the 10 lowest energy structures (Figure 5A). NOEs between the ribose of U_{35} and the H6 of U_{36} helped define their positions relative to each other. Their placement is consistent with that found in the X-ray crystallographic structure of lysyl-tRNA synthetase with cognate $tRNA^{Lys}$ wherein a phenylalanine intercalates between U_{35} and U_{36} (*53*).

At the pH 5.6, A^+_{38} is protonated and charged in the unmodified ASL^{Lys3}_{UUU} (*15*). Incorporation of t^6A_{37} does not alter the protonation of A^+_{38}. However, the negative charge contributed by the dissociated carboxylic acid of threonine would neutralize the positive charge of A^+_{38}. While the H1 proton of A^+_{38} is not directly observable, protonation of the N1 of the nucleobase is evident from the chemical shift change in H2 (*15*, *54*). An even clearer indicator of adenosine protonation is the upfield shift of the C2 resonance (*54*). As A_{38} became protonated with the lowering of the pH, its C2 resonance shifted upfield (see Supporting Information). Formation of an intraloop base pair between C_{32} and A^+_{38} and adjacent to the stem, could be responsible for stabilizing the RNA at low pH (Table 1) (*15*). Introduction of t^6A_{37} altered the C_{32}·A^+_{38} base-pairing geometry found in the unmodified ASL^{Lys3}_{UUU} (*15*). The threonyl group occupies the same space as U_{34} of the unmodified ASL^{Lys3}_{UUU} (Figure 6). To adapt to the t^6A modification, U_{34} is displaced away from t^6A_{37} and C_{32} is moved to accommodate U_{34} (Figure 6). Displacement of U_{34} by t^6A_{37} distorts the C_{32}·A^+_{38} base pair by shifting C_{32} out of alignment with A^+_{38}. The through space hydrogen bonding angles, A_{38}−N1−H1 to C_{32}−O2 and A_{38}−N6−H6.1 to C_{32}−N3 are 163° and 168°, respectively, for the unmodified ASL^{Lys3}_{UUU}. When t^6A_{37} is added, the hydrogen bonding angles decrease to 143° and 155°, an average of a 17° difference from the unmodified structure and 31° from being linear. It should be noted that this geometry of structure arises from an analysis of the average structure, and that no hydrogen-bonding constraints involving A_{38} were introduced in the calculations. When C_{32}·A^+_{38} was constrained to be hydrogen-bonded and repeated with the same restrain set, no new violations arose during the distance geometry phase of the modeling and after refinement there was little difference in energy distribution among the structures (data not shown).

Most significant to biological function, t^6A_{37} eliminates the canonical intraloop U_{33}·A_{37} hydrogen bond, displaces U_{34} and facilitates 3′-stacking of the loop. Because t^6A_{37} negates base pair formation in the ASL^{Lys3}_{UUU} loop no additional rearrangement of the bases need occur to accommodate the modifications of U_{34}, $mcm^5s^2U_{34}$, and the ms^2-derivative of t^6A_{37} (Figures 5 and 6). From these results and those of the preceding paper in this issue (*14*), we conclude that an open, structured loop is required for ribosomal binding. Ribosome binding cannot simply be an induced fit of the ASL, otherwise the unmodified ASL^{Lys3}_{UUU} would bind as well as the unmodified $ASL^{Lys1,2}_{CUU}$ (*14*, preceding paper in this issue). This not being the case, anticodon stem and loop domains are distinctive for unambiguous recognition of the tRNA by cognate aminoacyl-tRNA synthetase and for recognition of individual codons on the ribosome, yet share a similar architecture for ribosome binding. Modified nucleoside chemistry and structure impart just such a duality to ASL^{Lys3}_{UUU} and probably function similarly for other tRNAs.

ACKNOWLEDGMENT

A special thanks to Robert J. Cain whose initial studies demonstrated that this project was feasible. We thank Winnell Newman and Guihua Liu of the NCSU Nucleic Acids Facility for the synthesis and purification of the RNAs used in this study. We would also like to thank Robert J. Cain and Connie Yarian for editorial comments and Hanna Sierzputowska-Gracz of the NCSU NMR Facility for help in spectroscopy.

SUPPORTING INFORMATION AVAILABLE

Graph summarizing the translational diffusion experiments in D_2O at 25 °C, high-resolution DQF−COSY and HSQC spectra of ASL^{Lys3}-t^6A_{37}, and a superposition of three HSQC spectra highlighting the pH dependent shift of $A_{38}C2$. Coordinates of the 10 lowest energy structures and an average structure have been deposited in the Protein Data Bank with accession number 1feq. This material is available free of charge via the Internet at http://pubs.acs.org.

REFERENCES

1. Tsuchihashi, Z., and Brown, P. O. (1992) *Genes Dev*. 6, 511−9.
2. Jacks, T., Power, M. D., Masiarz, F. R., Luciw, P. A., Barr, P. J., and Varmus, H. E. (1988) *Nature* 331, 280−3.
3. Precup, J., and Parker, J. (1987) *J. Biol. Chem. 262*, 11351−5.
4. Hagervall, T. G., Pomerantz, S. C., and McCloskey, J. A. (1998) *J. Mol. Biol*. 284, 33−42.
5. Heurgue-Hamard, V., Mora, L., Guarneros, G., and Buckingham, R. H. (1996) *EMBO J. 15*, 2826−33.
6. Isel, C., Marquet, R., Keith, G., Ehresmann, C., and Ehresmann, B. (1993) *J. Biol. Chem. 268*, 25269−72.
7. Isel, C., Lanchy, J. M., Le Grice, S. F. J., Ehresmann, C., Ehresmann, B., and Marquet, R. (1996) *EMBO J. 15*, 917−24.
8. Auxilien, S., Keith, G., Le Grice, S. F., and Darlix, J. L. (1999) *J. Biol. Chem. 274*, 4412−20.
9. Dao, V., Guenther, G., Malkiewicz, A., Nawrot, B., Sochacka, E., Kraszewski, A., Everett, K., and Agris, P. F. (1994) *Proc. Natl. Acad. Sci. U.S.A. 91*, 2125−9.
10. Agris, P. F., Guenther, R., Ingram, P. C., Basti, M. M., Stuart, J. W., Sochacka E., and Malkiewicz, A. (1997) *RNA 3*, 420−8.
11. Agris, P. F., Söll, D., and Seno, T. (1973) *Biochemistry 12*, 4331−7.
12. von Ahsen, U., Green, R., Schroeder, R., and Noller, H. F. (1997) *RNA 3*, 49−56.
13. Ashraf, S. S., Sochacka, E., Cain, R., Guenther, R., Malkiewicz, A., and Agris, P. F. (1999) *RNA 5*, 188−94.
14. Yarian, C., Marszalek, M., Sochacka, E., Malkiewicz, A., Guenther, R., Miskiewicz., A., and Agris, P. F. (2000) *Biochemistry 39*, 13390−13395.
15. Durant, P. C., and Davis, D. R. (1999) *J. Mol. Biol. 285*, 115−31.
16. Ogilvie, K. K., Usman, N., Nicoghosian, K., and Cedergren, R. J. (1988) *Proc. Natl. Acad. Sci. U S A 85*, 5764−8.
17. Agris, P. F., Malkiewicz, A., Kraszewski, A., Everett, K., Nawrot, B., Sochacka, E., Jankowska, J., and Guenther, R. (1995) *Biochimie 77*, 125−34.
18. Gehrke, C. W., Kuo, K. C., McCune, R. A., Gerhardt, K. O., and Agris, P. F. (1982) *J. Chromatogr. 230*, 297−308.
19. Yarian, C. S., Basti, M. M., Cain, R. J., Ansari, G., Guenther, R. H., Sochacka, E., Czerwinska, G., Malkiewicz, A., and Agris, P. F. (1999) *Nucleic Acids Res. 27*, 3543−9.
20. Serra, M., and Turner, D. H. (1995) *Methods Enzymol. 249*, 242−61.
21. Stejskal, E. O., and Tanner, J. E. (1965) *J. Chem. Phys. 42*, 288−92.
22. Tanner, J. E. (1970) *J. Chem. Phys. 52*, 2523−6.
23. Lapham, J., Rife, J. P., Moore, P. B., and Crothers, D. M. (1997) *J. Biomol. NMR 10*, 255−62.
24. Yang, X., Sanghvi, Y. S., and Gao, X. (1997) *J. Biomol. NMR 10*, 383−8.
25. Piotto, M., Saudek, V., and Sklenar, V. (1992) *J. Biomol. NMR 2*, 661−5.
26. Kumar, A., Ernst, R. R., and Wuthrich, K. (1980) *Biochem. Biophys. Res. Commun. 95*, 1−6.
27. Macura, S., and Ernst, R. R. (1980) *Mol. Phys. 41*, 95−117.
28. Bax, A., and Davis, D. G. (1985) *J. Magn. Reson. 65*, 355−60.
29. Griesinger, C., Otting, G., Wüthrich, K., and Ernst, R. R. (1988) *J. Am. Chem. Soc. 110*, 7870−2.
30. Piantini, U., Sorensen, O. W., and Ernst, R. R. (1982) *J. Am. Chem. Soc. 104*, 6800−1.
31. Braunschweiler, L., Bodenhausen, G., and Ernst, R. R. (1983) *Mol. Phys. 48*, 535−60.
32. Mareci, T. H., and Freeman, R. (1983) *J. Magn. Reson. 51*, 531−5.
33. Sklenar, V., Miyashiro, H., Zon, G., Miles, H. T., and Bax, A. (1986) *FEBS Lett. 208*, 94−8.
34. Kellogg, G. W., Szewczak, A. A., and Moore, P. B. (1992) *J. Am. Chem. Soc. 114*, 2727−8.
35. Varani, G., and Tinoco, I., Jr. (1991) *J. Am. Chem. Soc. 113*, 9349−54.
36. Palmer, A. G., III, Cavanagh, J., Wright, P. E., and Rance, J. (1991) *J. Magn. Reson. 93*, 151−70.
37. Kay, L. E., Keifer, P., and Saarinen, T. (1992) *J. Am. Chem. Soc. 114*, 10663−5.
38. Guntert, P., and Wüthrich, K. (1992) *J. Magn. Reson. 96*, 403−7.
39. Wüthrich, K., Billeter, M., and Braun, W. (1983) *J. Mol. Biol. 169*, 949−61.
40. Varani, G., Aboul-ela, F., and Allain, F. H. T. (1996) *Prog. Nucl. Magn. Reson. Spectrosc. 29*, 51−127.
41. Gorenstein, D. G., (1984) *Phosphorus-31 NMR*: *Principles and Applications*, Academic Press, Florida.
42. Koshlap, K. M., Guenther, R., Sochacka, E., Malkiewicz, A., and Agris, P. F. (1999) *Biochemistry 38*, 8647−56.
43. Weiner, S. J., Kollman, P. A., Nguyen, D. T., and Case, D. A. (1986) *J. Comput. Chem. 7*, 230−53.
44. Reddy, P. R., Hamill, W. D., Jr., Chheda, G. B., and Schweizer, M. (1981) *Biochemistry 20*, 4979−86.
45. Reddy, P. R., Schweizer, M. P., and Chheda, G. B. (1979) *FEBS Lett. 106*, 63−6.
46. Várnagy, K., Jezowska-Bojczuk, M., Swiatek, J., Kozlowski, H., Sóvágó, I., and Adamiak, R. W. (1990) *J. Inorg. Biochem. 40*, 357−63.
47. Dewar, M. J. S., Bingham, R. C., and Lo, D. H. (1977) *J. Am. Chem. Soc. 99*, 4899.
48. Besler, B. H., Merz, K. M., and Kollman, P. A. (1990) *J. Comput. Chem. 11*, 431−9.
49. Parthasarathy, R., Ohrt, J. M., and Chheda, G. B. (1977) *Biochemistry 16*, 4999−5008.
50. Tewari, R. (1995) *Chem. Phys. Lett. 238*, 365−70.
51. Wijmenga, S. S., and van Buuren, B. N. M. (1998) *Prog. Nucl. Magn. Reson. Spectrosc. 32*, 287−387.
52. Kim S. H., Suddath F. L., Quigley G. J., McPherson A., Sussman J. L., Wang A. H., Seeman N. C., and Rich A. (1974) *Science 185*, 435−40.
53. Cusack S., Yaremchuk A., and Tukalo M. (1996) *EMBO J. 15*, 6321−34.
54. Sierzputowska-Gracz, H., Gopal, H. D., and Agris, P. F. (1986) *Nucleic Acids Res. 14*, 7783−801.

BI0013039